13th World Conference on Earthquake Engineering
Vancouver, B.C., Canada
August 1-6, 2004
Paper No. 2569

TIME-FREQUENCY PERSPECTIVES IN THE ANALYSIS AND INTERPRETATION OF GROUND MOTIONS AND STRUCTURAL RESPONSE

Tracy KIJEWSKI-CORREA[1], Ahsan KAREEM[2]

SUMMARY

Many Civil Engineering processes are characterized by nonstationary and nonlinear features that are often obscured in more traditional Fourier-based analysis schemes. As these representations provide an averaged-sense of frequency content, they do not distinguish noteworthy frequency components that are of short duration and high-intensity from those arising from persistent, low-amplitude features. The ability to differentiate these contributions is critical, as they can induce drastically different responses in a given structure, motivating this study's use of frameworks capable of resolving energy content with both frequency and time. In tandem with specified signal processing treatments, this study presents a suite of wavelet perspectives, from wavelet instantaneous frequency spectra (WIFS), which can track evolving frequency content, to instantaneous power spectra, which resolve the relative energy contributions of different frequency bands at "snapshots" in time, and time/frequency energy accumulation rates for recorded ground motions.

The utility of these tools is demonstrated in their application to ground motions from the Mexico City Earthquake (1985), highlighting the time-frequency characteristics of records from the Guerrero Array and Mexico City, as well as identifying the underlying relationship between frequency content at the two locations. The study also investigates the role of wavelets in analyzing seismic response, demonstrating that this transform can track the evolution of softening and even damage within a structure using a single recorded time history, by tracking the permanent reduction of modal frequencies marked by wavelet ridges. As such, this approach affords a potential damage indicator that does not require baseline frequency information.

INTRODUCTION

Undoubtedly, the Fourier Transform remains one of the most significant contributions to signal analysis and interpretation within the fields of Civil and Earthquake Engineering. However, it is important to note

[1] Rooney Family Assistant Professor, Structural DYNamics And MOnitoring (DYNAMO) Laboratory, Department of Civil Engineering & Geological Sciences, University of Notre Dame, Notre Dame, IN, USA. Email: tkijewsk@nd.edu
[2] Robert M. Moran Professor, NatHaz Modeling Laboratory, Department of Civil Engineering & Geological Sciences, University of Notre Dame, Notre Dame, IN, USA. Email: kareem@nd.edu

that stationarity becomes a stifling restriction of Fourier-based spectral analysis, particularly when analyzing highly transient events such as seismic ground motions. The inability to capture time-varying energy content within these traditional spectral frameworks has motivated the use of time-frequency transforms for the detection of nonstationary features in natural loading and the resultant response. One such transform actually has its roots in seismology applications: the wavelet. It was Morlet's work in reflection seismology that led him to propose sending shorter waveforms at high frequencies obtained by scaling a single function called a wavelet. At the same time, Grossman was working on coherent quantum states and realized the applicability of Morlet's idea to his field. The collaboration between these two led to the formalization of the continuous wavelet transform, known in French as *Ondelettes* [1]. Though these ideas were not new to mathematicians working in harmonic analysis and researchers in multi-scale image processing, the work of Grossman and Morlet, as well as the mathematician Meyer, brought together researchers from a variety of fields to unify the theory of wavelets. Therefore, it is only fitting to return to the seismic problem and particularly revisit it in the context of not only seismic ground motions, but also the resulting response to further develop the potential of wavelets discussed in Gurley & Kareem [2].

ANALYSIS PROCEDURE

Wavelet Theory

By breaking a signal down at every time step using a parent basis function of finite length, wavelets provide the ability to capture nonstationary features. The parent basis function is then scaled via dilations to generate a family of wavelets, with optimally adjusted resolutions based on the frequency being analyzed. Since detailed treatments of wavelet theory can be obtained from a number of texts, e.g. Mallat [3] and Chiu [4], only relevant details are presented herein for brevity. The continuous Wavelet Transform (CWT) is a linear transform that decomposes a signal $x(t)$ via basis functions that are simply dilations and translations of the parent wavelet $g(t)$ through the convolution with the signal according to

$$W(a,t) = \frac{1}{\sqrt{a}} \int_{-\infty}^{\infty} x(\tau) g^{*}\left(\frac{\tau - t}{a}\right) dt \tag{1}$$

where * denotes complex conjugate. Dilation by the scale, a, inversely proportional to frequency, represents the periodic or harmonic nature of the signal. The resulting wavelet coefficients, $W(a,t)$, represent a measure of the similitude between the dilated/shifted parent wavelet and the signal at time t and scale (frequency) a. The normalization by the root of scale insures that the integral energy given by the wavelet is independent of dilation.

Though there are countless parent wavelets used in practice, of both discrete and continuous form, this paper shall focus on the continuous wavelet transform using the Morlet wavelet [1], as its analogs to the Fourier transform make it quite attractive for harmonic analysis. These analogs are evident from the Morlet basis function

$$g(t) = e^{i\omega_o t} e^{-t^2/2} = e^{-t^2/2}\left(\cos(\omega_o t) + i\sin(\omega_o t)\right). \tag{2}$$

Essentially, the Morlet wavelet in Equation 2 is a Gaussian-windowed Fourier transform, with sines and cosines oscillating at the central frequency, f_o $(\omega_o = 2\pi f_o)$. Dilations of this temporally-localized parent wavelet then allow the "effective frequency" of this sine-cosine pair to change in order to match harmonic components within the signal. Further, there is a unique relationship between the dilation parameter of the transform, a, and the Fourier frequency, f, at which the wavelet is focused ($a = f_o/f$). The use of such a scaled basis function also implies that both the time and frequency resolutions of the wavelet transform are also scaled appropriately for the frequency being analyzed. The time (Δt) and frequency (Δf) resolutions of the wavelet transform are given by [4]

$$\Delta t = a\Delta t_g \qquad \text{and} \qquad \Delta f = \Delta f_g \,/\, a \tag{3 a, b}$$

and indicate that resolutions of the wavelet are simply scaled versions of the time (Δt_g) and frequency (Δf_g) resolutions of the parent wavelet and therefore depend upon the central frequency f_o chosen for the analysis.

Wavelet Representations

The application of Equation (1) to an arbitrary signal yields wavelet coefficients whose squared magnitude is representative of signal energy distributed in time and frequency (scale). This most basic representation is often referred to as the wavelet *scalogram*, *SG(a,t)*. However, these coefficients can also be viewed in a number of other formats depending on the perspective desired. The scalogram will appear as a color contour representation of energy in the time-frequency plane. These contours, when using parent wavelets such as the Morlet wavelet in Equation (2), have the tendency to “concentrate” at the frequency values associated with dominant harmonics in the signal, defining a series of curves called ridges that evolve with time. These ridges, whose extraction techniques are discussed in Carmona et al. [5], are locations where the frequency of the scaled wavelet coincides with the local frequency of the signal. These frequencies are defined as instantaneous frequencies (IF) for the signal. Thus a more precise representation of time-frequency energy content is obtained by retaining only the isolated ridges in the time-frequency plane. This perspective is termed by the authors as a *wavelet instantaneous frequency spectrum* (WIFS):

$$WIFS(a,t) = \begin{cases} SG(a,t)\big|_{a=a_r(t)} \\ 0\big|_{a\neq a_r(t)} \end{cases}. \tag{4}$$

The *marginal wavelet power spectrum,* also referred to as the *mean wavelet spectrum* [6] can be estimated by integration over the time variable as discussed in Perrier et al. [7], which when implemented for a signal of finite duration T, may be expressed as

$$S_{WT}(a) = \frac{2}{C_g}\left[\frac{1}{T}\int_0^T SG(a,t)dt\right] \tag{5}$$

where C_g is the *admissibility factor* or norm of the parent wavelet. The mean square value, or variance of an assumed zero mean signal, can be then determined from the wavelet marginal power spectrum by integrating over the range of scales

$$\sigma_{WT}{}^2 = \int_{a_1}^{a_n} S_{WT}(a)\frac{da}{a^2}. \tag{6}$$

Note that the limits of integration are defined in terms of the finite range of scales considered in the analysis and will identically capture the signal variance as $a_1 \rightarrow 0$ and $a_2 \rightarrow \infty$, equivalent to the theoretical expression in Mallat [3].

Wavelet measures of *energy accumulation* are also presented in this work. The energy accumulations in the frequency domain, denoted *E(f),* are determined by an integral operation at each frequency of the wavelet marginal spectrum, according to

$$E(f_i) = \int_{f_1}^{f_i} S_{WT}\left({f_o}/{f} \right) df \qquad \text{for } i=1, 2, .. n \tag{7}$$

for each of the *n* Fourier frequencies (scales) considered in the wavelet analysis. Similarly, a time analog to the marginal spectrum may be defined as

$$S_{WT}(t) = -\int_{f_1}^{f_n} SG\left({f_o}/{f}, t \right) df \ . \tag{8}$$

Energy accumulations in the time domain, denoted *E(t),* are then appropriately determined by

$$E(t_j) = \int_{t_1}^{t_j} S_{WT}(t) dt \qquad \text{for } j=1, 2, .. m \tag{9}$$

for each of the *j* discretely sampled time ordinates considered in the wavelet analysis. Rates of change or derivatives of each of these accumulation measures, with respect to frequency or time, denoted respectively as *dE(f)/df* or *dE(t)/dt*, and the maximum values of these accumulation rates will be of particular interest in subsequent discussions as they identify the arrival of significant events in time and frequency.

It should be noted that the assessment of the relative strength of a frequency component in a wavelet analysis should not be based on the amplitude of wavelet coefficients, but rather by the energy associated with that scale. This is necessary due to the multiresolution character of wavelets. Thus the relative contribution of various frequency components can be determined only by integrating the area under an instantaneous spectral peak. In this discussion, *instantaneous power spectra* will be examined as "snapshot" spectra associated with particular instants of time, achieved by plotting scalogram coefficients as a function of frequency for a specified time *t*. These instantaneous spectra have maxima at each instantaneous frequency component in the signal, denoted by IF_i. (A more detailed discussion of instantaneous frequency estimation techniques and their role in Civil Engineering analysis is provided in Kijewski-Correa [8] and summarized in Kijewski & Kareem [9]). Therefore, the relative contribution to the *instantaneous signal energy* at that time t_j from that frequency component is defined here as the ratio of the area under that particular spectral peak to the overall area under the instantaneous spectrum (time-localized variance)

$$\hat{E}_i(t = t_j) = \frac{\int_{f_{1,i}}^{f_{2,i}} SG\left({f_o}/{f}, t = t_i \right) df}{\int_{f_1}^{f_n} SG\left({f_o}/{f}, t = t_i \right) df} \ . \tag{10}$$

In this case, the limits of integration in the numerator are the frequencies associated with the initiation and termination of an individual spectral component.

Signal Processing Issues

As common to many continuous, infinite transforms, the application of Equation (1) to finite, discrete signals introduces a host of signal processing issues that must be addressed for meaningful results. These issues are particularly important in applications within Civil Engineering, as signals unique to this field tend to be more narrowband compared to their mechanical counter parts. As a result, Kijewski & Kareem [9] developed a framework in which these issues can be addressed for long-period signals: including the use of Equations (3a,b) to determine the appropriate central frequency for a given analysis, the use of a reflective padding scheme to remedy end effects, and a discretization scheme for selection of the scales at which to conduct the analysis. As discussed in Kijewski & Kareem [9], the parameters governing each of these considerations are the central frequency f_o, padding parameter β, and overlap factor OF, respectively.

In this paper, due to the short duration characteristics of seismic ground motions, a f_o = 1 Hz Morlet wavelet was first applied for more precise time resolution, followed by a detailed examination of the frequency content, achieved using a Morlet wavelet with f_o = 3 Hz. The use of such tiered analyses allows one to hone in on frequency details and then temporal details separately. Discretization of scales is accomplished according to the approach in Kijewski & Kareem [9] with OF = 1. These two analyses are referred to throughout the examples in this paper as the primary and secondary analyses, respectively. The structural response record is analyzed with central frequency of 2 Hz and a highly refined discretization (OF = 0.5). All signals are analyzed at scales corresponding to Fourier frequencies from 0.05 Hz to the Nyquist frequency. Dependent on the length of the record and the central frequency chosen, padding was provided using β = 2 or 3.

APPLICATIONS

Armed with an understanding of these signal processing issues and various wavelet visualizations, the analysis approach introduced here was extended to a number of measured earthquake ground motions and structural responses to earthquakes. The length of this paper does not permit discussion of results from all five major earthquake events studied in Kijewski-Correa [8], only the Mexico City earthquake is discussed here. It should be cautioned when viewing the following results that the associated time and frequency characteristics depend strongly on local soil conditions and should not be considered representative of the complete suite of seismic motions associated with the Mexico City event. This is then followed by an example concerning the response analysis of Sherman Oaks Building during the Northridge Earthquake (1994).

Mexico City Earthquake (1985)

This magnitude 8.1 earthquake that devastated Mexico City on September 19, 1985 occurred on the western coast of the Mexican peninsula. It had tremendous impacts upon the valley of Mexico City as a result of unique soil conditions, which amplified the low frequency components of the excitation. Though the frequencies affected varied from site to site within the city, the amplification was largely between 0.2 and 0.7 Hz. The concentrations of energy in the range of 0.2-0.6 Hz, being much higher than in previous quakes of comparable magnitude, led to heavy damage of structures in this period range [10]. To demonstrate the pronounced impacts of soil conditions, a nearfield record taken near the epicenter in the coastal regions of Mexico is first analyzed, recorded at Caleta de Campos, part of the Guerrero Array. To avoid confusion, this nearfield record will be referred to as the Guerrero MC (Mexico City) record in subsequent discussions. This coastal station had an epicentral distance of 27.1 km, making it well suited to capturing the nearfield characteristics of the quake. Subsequently, a free field record from the Mexico City valley, which typifies the low frequency amplification causing much of the damage in this quake, was also be analyzed. The nearfield Guerrero MC record is of considerable duration, although the peak ground accelerations are not as significant.

The primary and secondary wavelet scalograms and WIFS for the Guerrero MC nearfield record are presented in Figure 1. The enhanced temporal resolution of the primary analysis isolates three energetic bursts: one event between 10 and 15 s and the other between 1 and 1.75 Hz, followed by strong shaking between 2 and 3 Hz accompanied by a low frequency component near 20 s. A slight burst of energy near 21 s is also apparent. From the scalogram and the associated WIFS, there is a collection of energy over the first 30 s and spanning a wide range of frequencies. Note in the primary WIFS that dominant ridges surface near 1.75 Hz and 0.5 Hz, the latter particularly in the vicinity of the strong shaking at 20 s. These are flanked by intermittent contributions in the high frequency range. The refined frequency resolution in the secondary analysis further affirms the richness of energy and the concentrations near 2.55 Hz and 1.75 Hz around the 20th second, as well as the precursor to the strong shaking at 12 s. Though diminished in magnitude by virtue of the dilated temporal windows, a residual low frequency component is still apparent and further affirmed by the ridges in the secondary WIFS. The secondary scalogram does give a better perspective on the intermittence of high frequency components within the record, though the resolutions in the low frequency range lead to a dilation of the time windows evident by the elongated bands in the low frequency domain. The fluctuations of these high frequency ridges become more readily apparent in the secondary WIFS, as does the downshift of midrange frequencies and upshift of the low frequencies approaching the strong shaking near the 20th second.

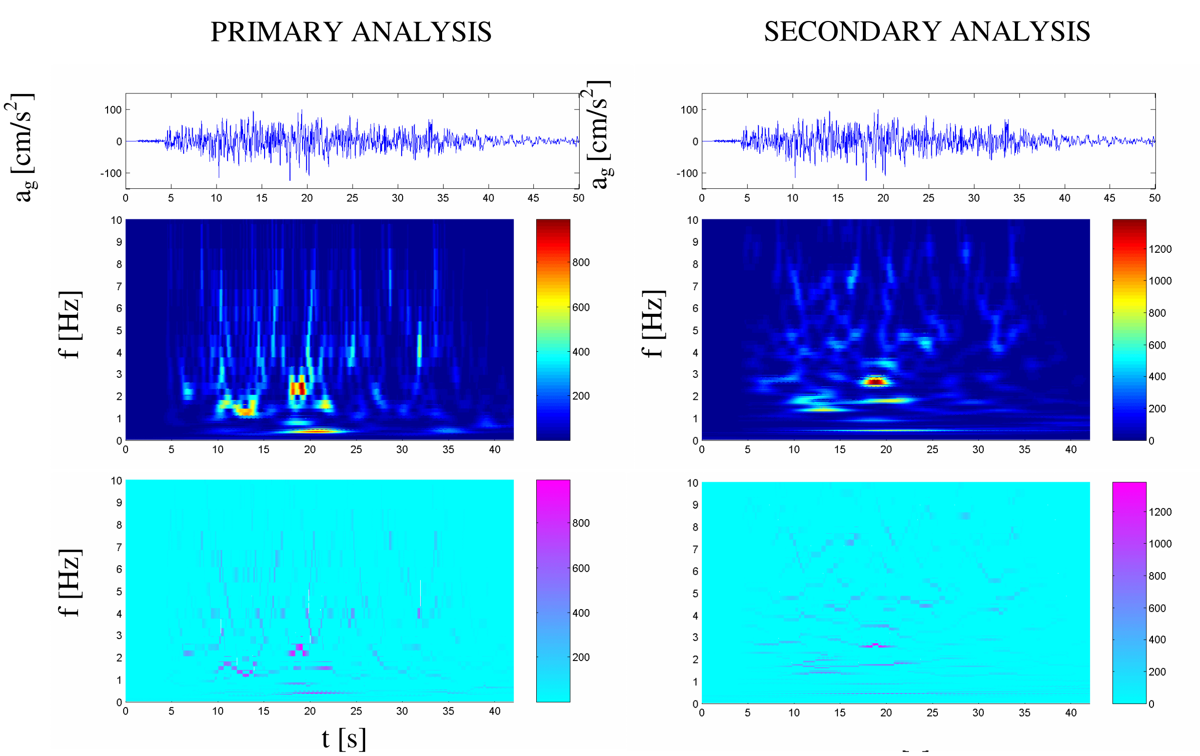

FIGURE 1. Guerrero MC nearfield ground motion, wavelet scalogram and WIFS (top to bottom) for primary (left) and secondary analyses.

Figure 2 presents the energy accumulation rates in frequency and time for the primary and secondary analyses. As the figure demonstrates, the primary analysis smoothes out many of the details of the energy accumulation with frequency. The rate of change of energy accumulation in frequency, shown in Figure 3, offers a more clear indication of the explicit frequency components of the quake.

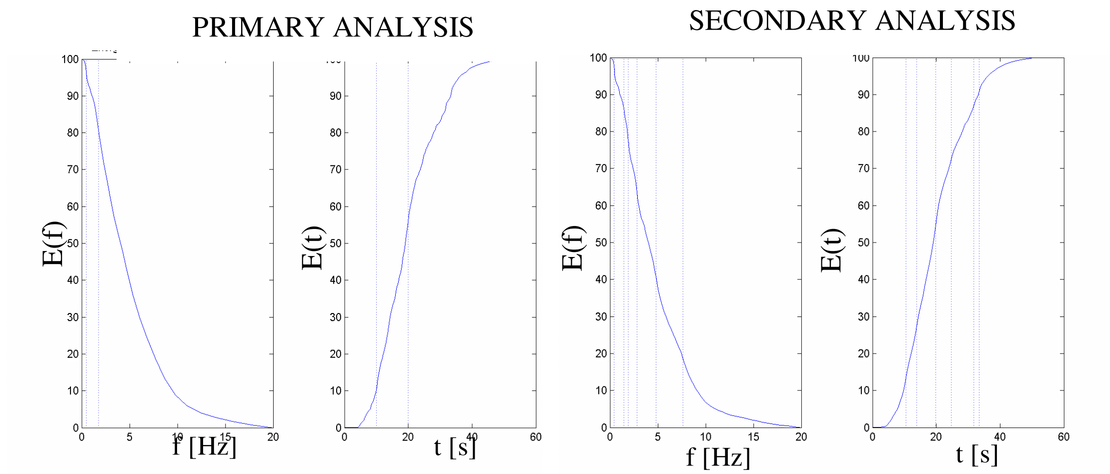

FIGURE 2. Energy accumulation in frequency domain and time domain for primary (left) and secondary analysis of Guerrero MC nearfield record.

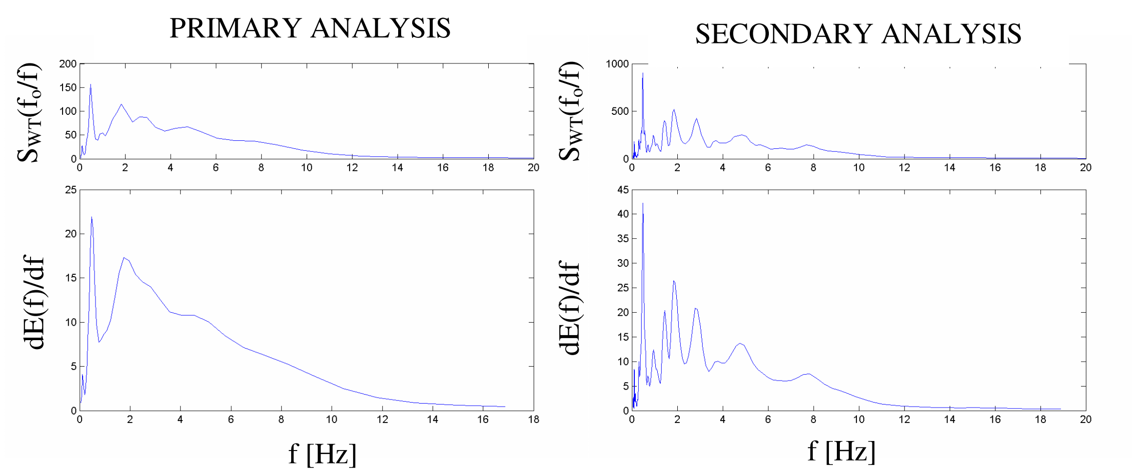

FIGURE 3. Wavelet marginal spectrum and rate of change of energy accumulation in frequency domain for primary (left) and secondary analysis of Guerrero MC nearfield motion.

Due to the compromised frequency resolution in the primary analysis, the rate of change of energy accumulation in the frequency domain in Figure 3 is only able to isolate a very energetic component at 0.47 Hz followed by a more broadband contribution peaking at 1.76 Hz. The broadness of this peak implies that a bulk of the influx of energy into the system comes from frequencies in this vicinity. The primary analysis affirms that 79% of the energy associated with this nearfield motion is associated with frequencies greater than 1.8 Hz. Despite the sharp increase in energy accumulation near 0.5 Hz, the nearfield Guerrero MC record was found to contain only approximately 3% of its energy at frequencies under 0.5 Hz. The secondary analysis provides some additional details on the participating frequencies in the 2 Hz range. It should be noted that the resolutions low frequency resolutions of a wavelet analysis are superior to that of a Fourier Analysis due to the multiresolution nature of the transform. Thus it is well-suited for the investigation of frequency content in the ranges of interest to Civil Engineering.

The peaks associated with influxes of energy into the system can be traced back to the accumulation plot in Figure 2 to isolate specific contributions, as shown by the dotted vertical lines. This analysis reflects that approximately 6% of the signal energy lies at or below 0.5 Hz. Though several frequency components less than 2 Hz are shown to provide increases to cumulative energy in the signal, a total of approximately 20% of the nearfield signal resides less than 2 Hz. Another 20% resides at frequencies above 7.62 Hz, consistent with the findings from simulation studies, which found that the Guerrero gap might produce energy at a wide distribution of frequencies including high frequency motions [11]. The temporal energy accumulation plots in Figure 2 indicate that the ten seconds of shaking from 14 to 24 s brings over 46% of the signal energy, isolating the most energetic component near 20 s.

The analyses of the instantaneous spectra taken at critical moments in the nearfield event are shown in Figure 4 along with the relative energy contributions in Table 1 for the secondary analysis only, as the secondary analysis provides added detail in the frequency domain. It is important to note that in the four spectral snapshots, the contributions near 0.5 Hz remain on the order of but a few percent of the total energy at each time. Instead, the majority of energy resides in the higher frequency bands beyond 2 Hz. The most energetic component of this record is in the vicinity of 20 s and is represented by the second spectral "snapshot" carrying five distinct frequency components under 4 Hz, responsible for nearly half the energy at this time. Moving away from the most energetic moment in the shaking, the emphasis on the low frequencies diminishes and the energy again moves toward the higher frequencies beyond 4 Hz, affirming the ability of the Guerrero gap to produce such high frequency excitations. The simultaneous presence of both high and low frequency shaking is a unique characteristic of the Mexico City event in comparison to other records studied in Kijewski-Correa [8]. Despite the decided shift toward the higher frequencies, the persistent presence of the low frequency contributions at 0.5 Hz should be noted, as they will play a critical role once the seismic waves arrive in the Mexico City valley. The images in Figure 4 speak again to the nonstationarity inherent in seismic ground motions.

TABLE 1: Relative contributions of each component to instantaneous spectra for Guerrero MC nearfield record in secondary analysis.

t_j [s]	E(t) [%]	IF_1 [Hz]	$\hat{E}_1(t_j)$ [%]	IF_2 [Hz]	$\hat{E}_2(t_j)$ [%]	IF_3 [Hz]	$\hat{E}_3(t_j)$ [%]	IF_4 [Hz]	$\hat{E}_4(t_j)$ [%]	IF_5 [Hz]	$\hat{E}_5(t_j)$ [%]
10.3	10	0.49	2.2	1.41	6.8	1.87	13.5	4.03*	33.2	7.05	36.3
20.0	47	0.49	4.91	0.95	4.02	1.93	9.48	2.78	17.3	3.70	13.1
24.7	70	0.49	6.05	No component		4.69	34.7	5.87	11.9	9.14	24.9
33.5	85	0.56	4.50	1.41	5.86	2.45	3.80	5.08	21.6	8.23	46.4

*midpoint of wide band energy distribution.

The collapse of a number of high-rise dwellings in the Mexico City earthquake emphasized the significance of site conditions in enhancing seismic risk, as it was observed that, at some locations in and near Mexico City, components in the vicinity of 0.5 Hz were dramatically amplified. Such amplification was not evident in coastal records, as shown in the preceding analysis and in Singh et al. [12]. In fact, ground motion at the lakebed sites in Mexico City were amplified nearly 75 times in the vicinity of 0.5 Hz

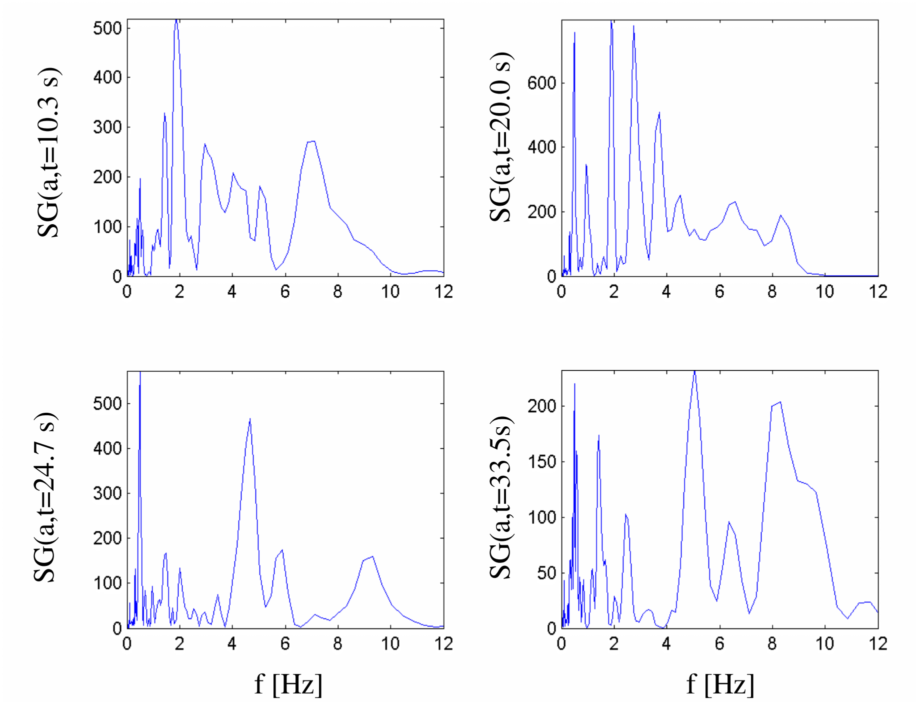

FIGURE 4. Wavelet instantaneous spectra taken at critical time steps in the Guerrero MC nearfield event for secondary analysis.

in comparison to the costal sites of equal distance from the source [12]. To demonstrate the dramatic amplification of the low frequency component, a free field record from the Mexico City Valley is analyzed by the aforementioned analysis techniques. Upon comparing the farfield time history in Figure 5, recorded in Mexico City, with the nearfield Guerrero MC time history in Figure 1, the regular periodic characteristic of the farfield record and the elongation of period are immediately evident. An inspection of the energy accumulation rates in the frequency domain (Figure 6) demonstrate the amplification of the low frequency energy of the event that is largely credited with the heavy damage to structures of comparable period, as noted in the post-disaster surveys of Mexico City. A strong amplification of the 0.49 Hz component is apparent with only a slight presence of energy beyond 1 Hz. Though this 0.5 Hz component was present in the coastal Guerrero MC record analyzed previously, the local site conditions clearly amplified this component of the shaking far above all others.

The rate of change in the frequency domain (not shown), peaks at 0.47 Hz, as can be inferred from the accumulation plot in Figure 6 that has a steep descent in this vicinity. From this plot, it is demonstrated that 80% of the energy at this site comes from frequencies between 0.37 and 0.67 Hz. An additional 10% of the energy is associated with frequencies less than 0.37 Hz. The rate of change of energy accumulation in the time domain is actually more insightful, isolating the three pulses in the quake at 42.5s, 50.4 and 58.5 s, which happen to be most energetic. Relaying this information to the energy accumulation, it is demonstrated that one-quarter of the signal energy arrives with this main pulse. To determine the frequency content of the quake at these various time intervals, several instantaneous spectra were assembled (not shown here). At each of the time steps, a single component at 0.49 Hz dominates, with approximately 98% of the instantaneous signal energy at that particular time interval.

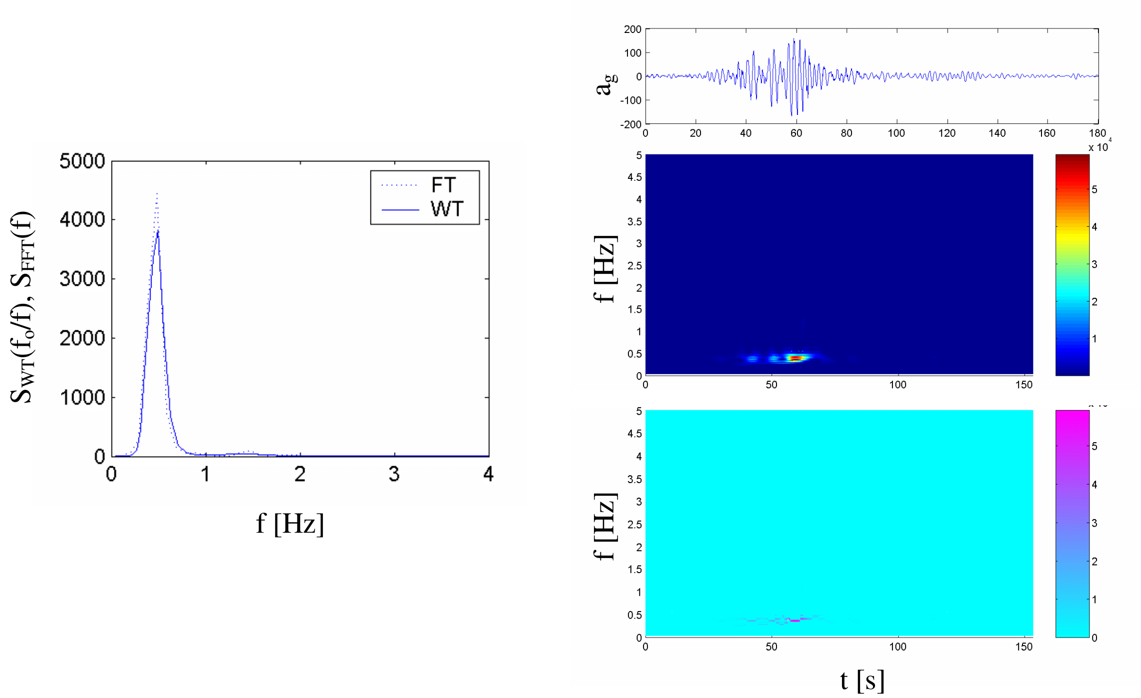

FIGURE 5. Comparison of Fourier spectrum and wavelet marginal spectrum (left) for Mexico City farfield ground motion with wavelet scalogram and WIFS (right, top to bottom)

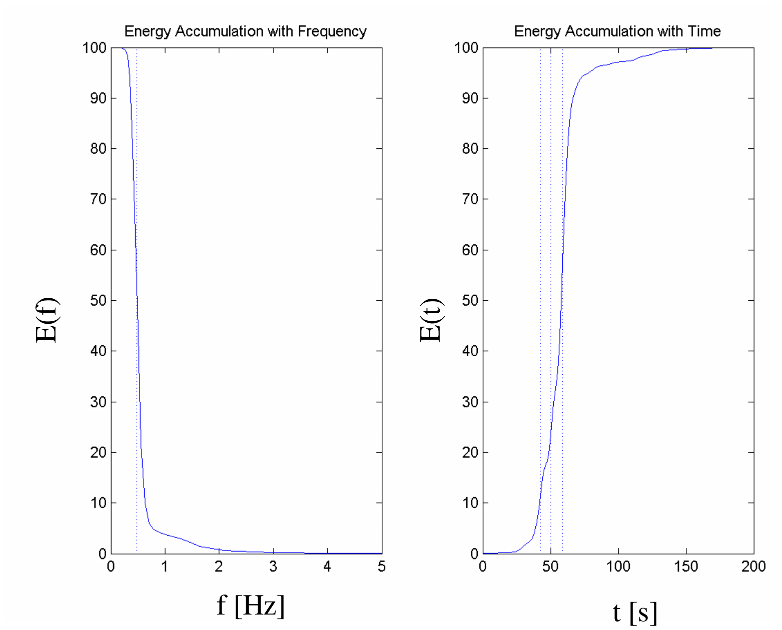

FIGURE 6. Energy accumulation in frequency and time for Mexico City farfield ground acceleration.

Seismic Response of Sherman Oaks Building

The previous analyses have highlighted the wavelet's ability to capture the nonstationary characteristics of earthquakes and reveal the evolution of frequency content with time. Similar and more physically meaningful insights for Civil Engineers can be obtained by applying this tool for the analysis of structural responses under these highly nonstationary events. To demonstrate the ability of the wavelet to capture nonstationary characteristics of structural response, consider the roof level acceleration of a 13-story commercial building (Sherman Oaks), along its longitudinal (E-W) axis during the 1994 Northridge earthquake. The measured acceleration is shown in Figure 7a. The resulting marginal spectrum and its Fourier counterpart are shown in Figure 7b. From this spectral representation, it appears that the response is dominant in the first mode near 0.38 Hz, accompanied by lesser contributions from a second mode at 1.17 and third mode at 2.34 Hz. The irregular shape of the wavelet marginal spectral peak in the first mode suggests the presence of nonlinearity. While the wavelet and Fourier representations are in good agreement in identifying the modes and their relative contributions, this detail in the fundamental mode is obscured by a comparable Fourier analysis. The wavelet spectrum further identifies the total energy of the system more accurately, with a standard deviation of 56.5 cm/s^2 verses the Fourier estimate of 60.0 cm/s^2, in good agreement with standard deviation of the signal itself (56.6 cm/s^2). Thus, overall energy content is well represented by Fourier Transforms, though all temporal information is completely lost.

The wavelet scalogram in Figure 7c preserves these evolutionary features, identifying two bursts of energy after the tenth and thirty-fifth seconds. As evident in the time series in Figure 7a, only the former large-amplitude response includes the two higher modes. An extraction of wavelet ridges produces the wavelet instantaneous frequency spectrum in Figure 7d. The ridges, though fainter for the higher frequency modes, manifest distinct fluctuations and an apparent softening of the fundamental ridge. Figure 7e zooms in on the third mode, darkening the plot and showing a hardening with the strong shaking, followed by a decrease in stiffness. The contributions of this mode are relatively isolated and manifest only with the strong shaking of the first 15 s. The second mode is present in both major shaking events, and when amplified and darkened in Figure 7f echoes a similar characteristic of softening, again reaching a minimum stiffness following the major pulse near 10s. The dominant low frequency ridge in Figure 7g begins at a plateau near 10 s and then softens in the subsequent 10 s, manifesting some slight hardening during the second event, which primarily affects this lowest mode. It is apparent that by the conclusion of the shaking, this structure's fundamental period has softened, a potential indicator of some permanent damage in the structure. Interestingly, a comparison of the structural frequencies obtained through testing after the quake with some estimates taken before the quake may have detected this softening. However, without a baseline for comparison, the frequencies identified after the quake shed little light. On the other hand, the wavelet analysis allows the determination of frequency throughout the shaking, so that one record alone can be used to document the onset of softening. In this context, wavelet-based analysis provides an attractive framework for structural health monitoring in the absence of such baseline data, which may not be available for most buildings.

The energy accumulation plots in Figure 8 reflect that energy is strongly accumulated near 0.347 Hz, corresponding to the first mode of the structure. Note that the accumulation in the frequency domain plateaus at three distinct points, readily identifying the three modes and their relative contributions. The third mode contributions are quite scarce (less than 10%), while the second mode contributes 10-15% of the total energy and the first mode is responsible for nearly 70% of the total signal energy, as expected.

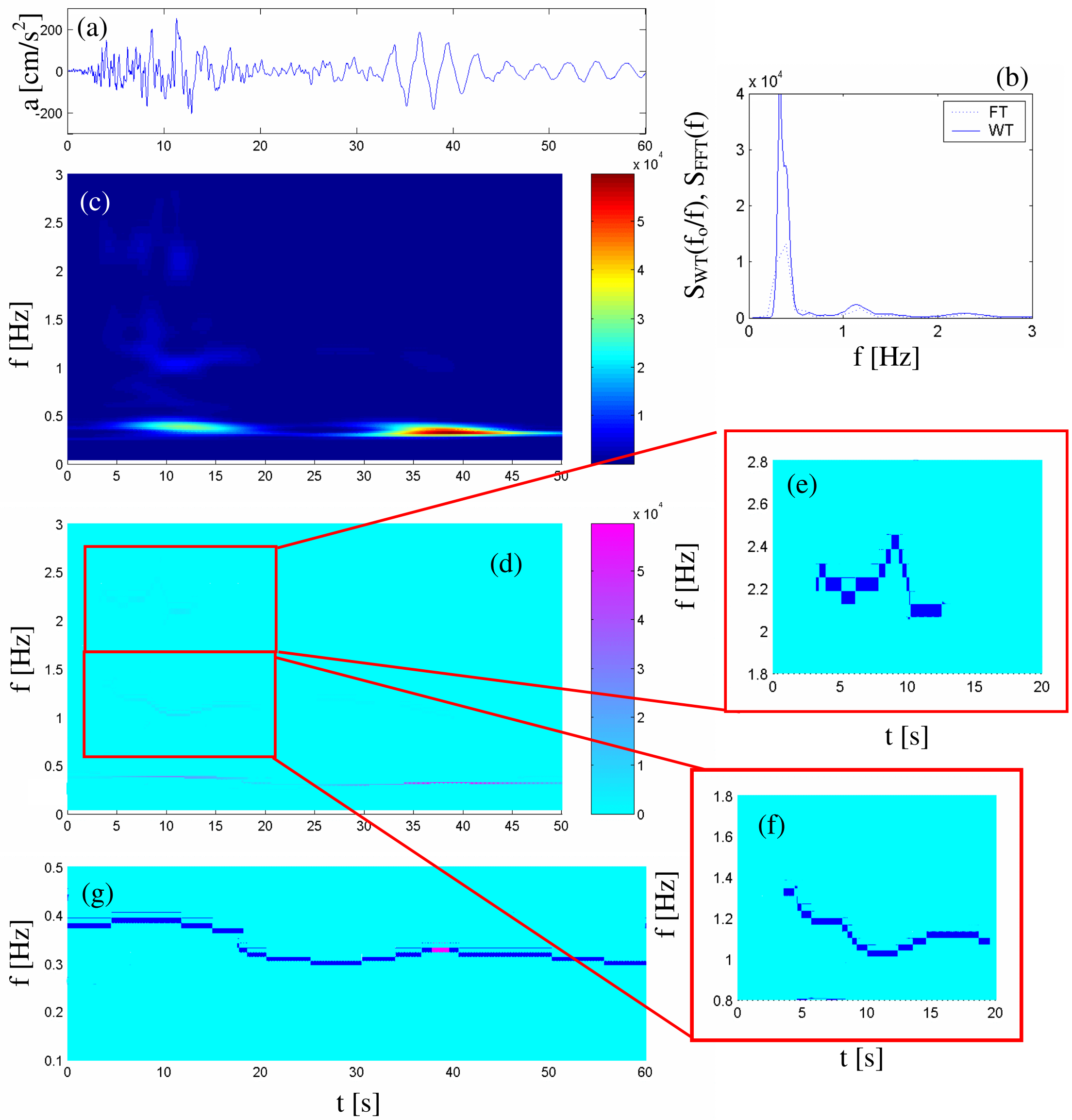

FIGURE 7. (a) Recorded structural response to Northridge ground motion, (b) Fourier and wavelet marginal spectra; (c) scalogram; (d) WIFS; (e) zoom of third mode ridge; (f) zoom of second mode ridge; (g) zoom of fundamental mode ridge

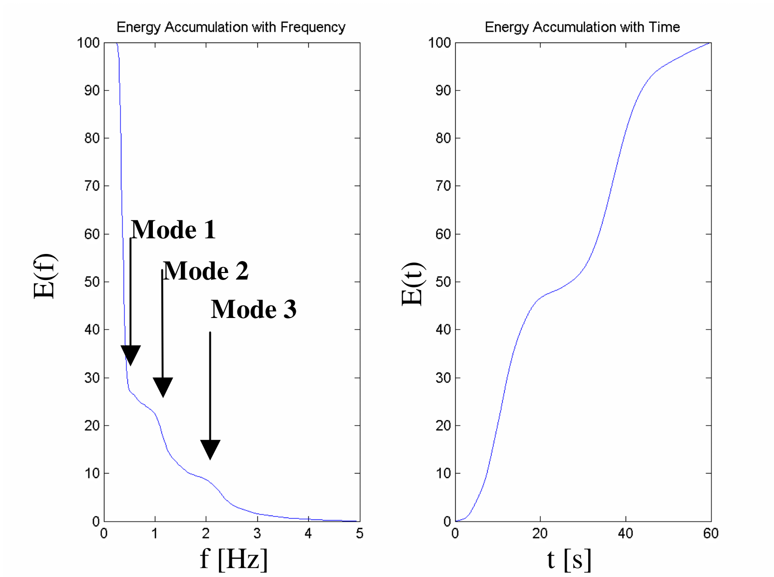

FIGURE 8. Energy accumulation in frequency domain and time domain for Sherman Oaks building under Northridge earthquake.

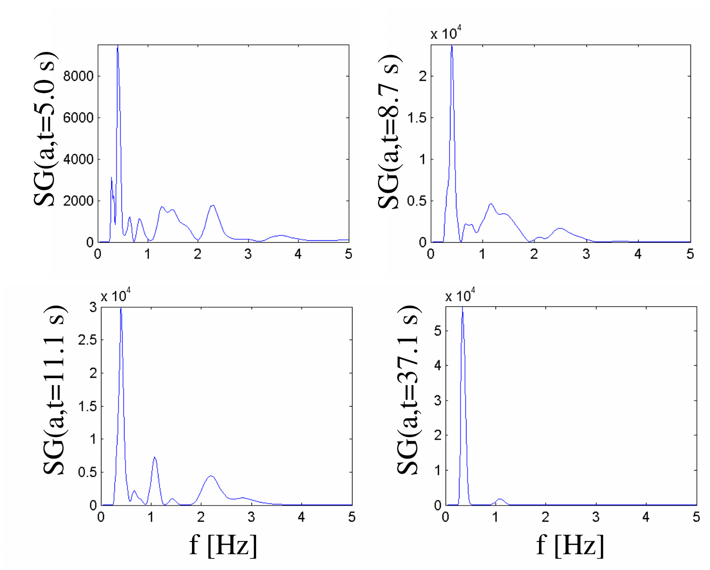

FIGURE 9. Wavelet instantaneous spectra taken at critical time steps in the Sherman Oaks building response in the Northridge earthquake.

The spectral "snapshots" of the energy distribution at distinct points within the response time history is provided in Figure 9 The first spectrum is associated with the plateau region in the rate of change in energy accumulation with time (Figure 8). This is a region where the rate of energy accumulation held relatively steady prior to strong shaking. At this time, all three modes appear to be present, though the two higher modes are sharing energy over a broad range of frequencies. The side lobes on the fundamental spectral peak indicate the presence of additional adjacent frequencies that could indicate nonlinearity within that mode. Note also the surfacing of a fourth, high frequency mode. The relative energy contributions from these modes are listed in Table 2. The next two spectra are associated with peaks in the early strong shaking. At 8.7 s, there is a relatively larger contribution from frequencies in the vicinity of the second mode, diminishing the influence of the third mode. At 11.1 s, the energy has shifted dominantly towards the first mode coupled with a band of energy near the third mode. The last spectrum is associated with the final significant response within the structure. As evidenced previously, this response is dominantly in the first mode, as evidenced by Table 2, with a minor second mode contribution. The more detailed investigations of energy distribution with time, provided in the instantaneous spectra, indicate that the energy is more prominently associated with the higher modes in the first 9 s of the event. Even at 11.1 s, despite the surging first mode response, there is still a strong contribution in the vicinity of the third mode. It is only in the decline in energy accumulation rates that the first mode overwhelmingly dominates the response. Again it should be noted that the Fourier perspective cannot reflect the intermittent participation of higher modes in the overall structural response.

TABLE 2: Relative contributions of each component to instantaneous spectra for Sherman Oaks building In Northridge earthquake.

t_j [s]	IF_1 [Hz]	$\hat{E}_1(t_j)$ [%]	IF_2 [Hz]	$\hat{E}_2(t_j)$ [%]	IF_3 [Hz]	$\hat{E}_3(t_j)$ [%]
5.0	0.40	32.9	1.38	28.4	2.28	19.5
8.7	0.42	40.7	1.13	44.5	2.50	13.4
11.1	0.42	50.6	1.08	17.3	2.20	31.0
37.1	0.34	93.7	1.10	5.8	No component	

CONCLUSIONS

Many Civil Engineering processes are characterized by nonstationary and nonlinear features that are often obscured in more traditional Fourier-based analysis schemes. As these representations provide an averaged-sense of frequency content, they do not distinguish noteworthy frequency components that are of short duration and high-intensity from those arising from persistent, low-amplitude features. The ability to differentiate these contributions is critical, as they can induce drastically different responses in a given structure. The specific examples of wavelet analysis of seismic ground motions and the associated response of Civil Engineering structures presented here highlight the ability of time-frequency transforms to uncover intermittent energy contributions through wavelet scalograms and instantaneous frequency spectra that characterize not only intermittent frequency components but also their relative contributions at specific stages of an event. The ability to detect and model nonlinear characteristics is particularly important for seismic analysis, where large amplitude response and structural damage can induce frequency variations and the participation of higher modes in the response that would be obscured in traditional Fourier analyses. The wavelet's ability to provide a description of such nonlinear and nonstationary features makes it an effective tool for response analysis and simulation.

ACKNOWLEDGEMENTS

The authors gratefully acknowledge NSF Grants CMS 00-85109 and CMS 03-24331, the NASA Indiana Space Grant, and the Center for Applied Mathematics at the University of Notre Dame.

REFERENCES

1. Grossman A, Morlet, J. “Decomposition of Hardy functions into square integrable wavelets of constant shape.” SIAM Journal of Mathematical Analysis 1984; 15(4): 723-736.
2. Gurley K, Kareem A. “Application of wavelet transforms in earthquake, wind, and ocean engineering.” Engineering Structures 1999; 21: 149-167.
3 Mallat S. “A wavelet tour of signal processing.” San Diego: Academic Press, 1998.
4. Chui CK. “Wavelet analysis and applications: an introduction to wavelets. vol. 1.” San Diego: Academic Press, 1992.
5. Carmona R, Hwang WL, Torresani B. “Practical time-frequency analysis.” San Diego: Academic Press, 1998.
6. Lewalle J. “Applications of continuous wavelets to data analysis, part I: wavelets without lemmas.” Von Karman Institute for Fluid Dynamics, Lecture Series 1998-06, Advanced Measurement Techniques, April 6-9, 1998.
7. Perrier V, Philipovitch T, Basdevant C. “Wavelet spectra compared to Fourier spectra.” Journal of Mathematical Physics 1995; 36(3): 1506-1519.
8. Kijewski-Correa T. “Time-frequency perspectives in system identification: from theory to full-scale measurements.” University of Notre Dame: PhD Dissertation, Department of Civil Engineering & Geological Sciences, 2003.
9. Kijewski T, Kareem A. “Wavelet transforms for system identification: considerations for civil engineering applications.” Computer-Aided Civil and Infrastructure Engineering 2003; 18: 341-357.
10. Jennings PC, Sanchez-Sesma FJ. “Working group conclusions on strong ground motion.” Bertero VV, Editor. Lessons learned from the Mexico City earthquake. El Cerrito, CA: EERI, 1989: 2-3.
11. Jennings PC, Kanamori H, Helmberger D, Clayton R, Singh S, Mena E, Astiz L. “Estimation of future strong ground motions in Mexico City.” Bertero VV, Editor. Lessons learned from the Mexico City earthquake. El Cerrito, CA: EERI, 1989: 15-17.
12. Singh SK, Mena E, Castro R. “Some aspects of source characteristics of the 19 September 1985 Michoacan earthquake and ground motion amplification in and near Mexico City from strong motion data (abstract).” Bertero VV, Editor. Lessons learned from the Mexico City earthquake. El Cerrito, CA: EERI, 1989: 39-40.